Crystal Structure and Theoretical Analysis of Green Gold $Au_{30}(S\text{-}tBu)_{18}$ Nanomolecules and Their Relation to $Au_{30}S(S\text{-}tBu)_{18}$

Amala Dass,*[,†] Tanya Jones,[†] Milan Rambukwella,[†] David Crasto,[†] Kevin J. Gagnon,[‡] Luca Sementa,[§] Martina De Vetta,[∥] Oscar Baseggio,[∥] Edoardo Aprà,[⊥] Mauro Stener,[∥] and Alessandro Fortunelli[§]

[†]Department of Chemistry and Biochemistry, University of Mississippi, Oxford, Mississippi 38677, United States

[‡]Advanced Light Source, Lawrence Berkeley National Laboraotry, 1 Cyclotron Road, Berkeley, California 94720, United States

[§]CNR-ICCOM, Consiglio Nazionale delle Ricerche, Pisa I-56124, Italy

[∥]Dipartmento di Scienze Chimiche e Farmaceutiche, Università di Trieste, Trieste I-34127, Italy

[⊥]Environmental Molecular Sciences Laboratory, Pacific Northwest National Laboratory, P.O. Box 999, K8-91, Richland, Washington 99352, United States

Supporting Information

ABSTRACT: We report the complete X-ray crystallographic structure as determined through single-crystal X-ray diffraction and a thorough theoretical analysis of the green gold $Au_{30}(S\text{-}tBu)_{18}$. While the structure of $Au_{30}S(S\text{-}tBu)_{18}$ with 19 sulfur atoms has been reported, the crystal structure of $Au_{30}(S\text{-}tBu)_{18}$ without the μ_3-sulfur has remained elusive until now, though matrix-assisted laser desorption ionization mass spectrometry (MALDI-MS) and electrospray ionization mass spectrometry (ESI-MS) data unequivocally show its presence in abundance. The $Au_{30}(S\text{-}tBu)_{18}$ nanomolecule not only is distinct in its crystal structure but also has unique temperature-dependent optical properties. Structure determination allows a rigorous comparison and an excellent agreement with theoretical predictions of structure, stability, and optical response.

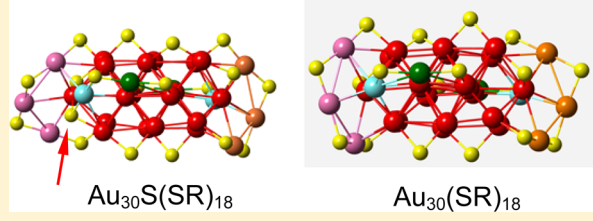

INTRODUCTION

Gold−thiolate nanomolecules, $Au_n(SR)_m$ are compounds with a fixed number n of gold atoms which are stabilized by passivating organic thiolate ligands m.[1] For instance, $Au_{25}(SR)_{18}^{-1,0}$, $Au_{38}(SR)_{24}$, and $Au_{144}(SR)_{60}$ are some of the most commonly studied nanomolecules, with size-dependent and unique chemical and physical characteristics.[2] Griffin and co-workers and others showed that self-assembled monolayers on a Au(111) substrate with mixed *tert*-butanethiol and *n*-octadecanethiol ligands revealed less densely packed monolayers (SAMs) with an increasing amount of *tert*-butanethiol, demonstrating that the bulkiness of the thiolate ligand modifies the packings of the SAMs.[3] Less common nanomolecules such as Au_{30}, Au_{39}, Au_{41}, Au_{65}, and other clusters have in fact been reported,[4] synthesized using sterically hindered bulky ligands. Aromatic thiolate ligands have also been shown to lead to uncommon altered cluster sizes.[5] Aromatic thiols introduce an additional complication as aromaticity and bulkiness are coupled in an intricate way, so that it is not possible to attribute the changes in geometric and electronic structure to bulkiness only. Because of this complex panorama, structural and geometric studies are highly reliant on the identification of crystallographic structure of the nanomolecules.

In this study we follow this line of research. We focus on a specific compound, $Au_{30}(S\text{-}tBu)_{18}$, green gold[6]—which had been identified so far only through mass spectrometry (MALDI-MS) and electrospray ionization mass spectrometry (ESI-MS)[6] but whose crystallography structure had remained elusive until now—and determine its crystallographic data. Its properties can be so thoroughly compared with that of a homologous $Au_{30}S(S\text{-}tBu)_{18}$ compound, whose structure had been previously reported,[7] thus providing an in-depth analysis on the composition, electronic, optical, and chiroptical properties. In addition to reporting the first crystallographic structure of the $Au_{30}(S\text{-}tBu)_{18}$ nanomolecule in two distinct packing structures (space groups $P2_1/n$ and P-1), determined through the use of single-crystal X-ray diffraction, we detail the unique temperature-dependent optical properties of $Au_{30}(S\text{-}tBu)_{18}$ and compare these optical properties with theoretical predictions obtained using time-dependent density-functional theory (TDDFT). We note that the $Au_{30}(S\text{-}tBu)_{18}$ presented here is an all-thiolate protected nanomolecule with a green color.[6] An earlier report in the literature on green gold[8] is unrelated to this work and refers to a water-soluble $Au{:}PR_3$ compound with an approximate atom count of 75 gold atoms, $Au_{\sim 75}$.

RESULTS AND DISCUSSION

$Au_{30}(S\text{-}tBu)_{18}$ was synthesized in a one-pot THF method (see Experimental Section for details), and crystallization was

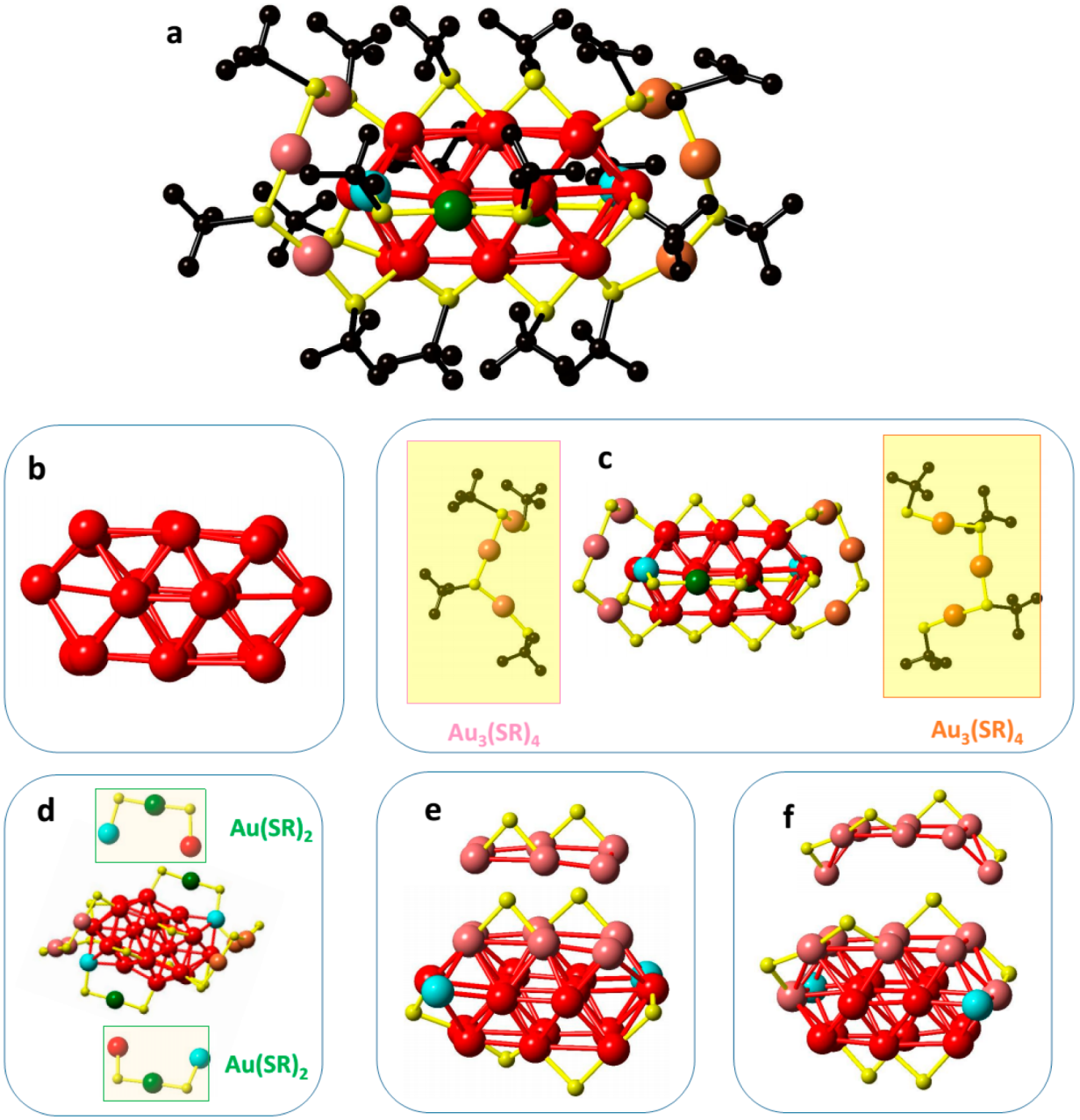

Figure 1. Single-crystal XRD structure of $Au_{30}(S\text{-}tBu)_{18}$. (a) Total structure of $Au_{30}(S\text{-}tBu)_{18}$ (hydrogen atoms are omitted for clarity). (b) Au_{20} skeleton showing an interpenetrating bicuboctahedral core geometry. (c) $Au_{30}S_{18}$ geometry showing the two trimeric [−SR−Au−SR−Au−SR−Au−SR−] units, highlighted in the red boxes as the inset/ (d) $Au_{30}S_{18}$ geometry showing the two monomeric [−SR−Au−SR−] units, highlighted in the red box as the inset (carbon atoms are omitted in (c) and (d) for clarity). (e and f) The positions of the rest of the SR groups on the Au_{22} bicuboctahedral substructure.

performed via hexane vapor diffusion into a toluene solution of $Au_{30}(S\text{-}tBu)_{18}$. Small green-needle-like crystals were obtained after 4−7 days. These needle-like crystals are different than the rhombic-shaped plate-like crystals of $Au_{30}S(S\text{-}tBu)_{18}$.

Experiment: Structure. Figure 1a presents the total structure of the bicuboctahedron $Au_{30}(S\text{-}tBu)_{18}$ cluster, which crystallizes in the space group $P2_1/n$. The structure was refined to a resolution of 1.06 Å and to a value of R_1 = 10.93%. Figure 1b shows the Au_{30} skeleton with an interpenetrating bicuboctahedral core. The geometry, shown in Figure 1c, represents the Au-SR staples and bond structures of $Au_3(SR)_4$. Figure 1d represents the $Au_{30}S_{18}$ geometry, highlighting the two monomeric [−SR−Au−SR−] units. The structure of $Au_{30}(S\text{-}tBu)_{18}$ is a prolate configuration composed of a Au_{20} polytetrahedral core with its tips symmetrically capped by two $Au_3(S\text{-}tBu)_4$ units and its central body wrapped by four $Au(S\text{-}tBu)_2$ units and two S-*t*Bu groups in bridge sites between two Au atoms, see Figure 1. A second synthesis resulted in a different crystal structure containing the same bicuboctahedron $Au_{30}(S\text{-}tBu)_{18}$ cluster. It crystallizes in the space group *P*-1 and is refined to a resolution of 0.81 Å and to a value of R_1 = 5.26%. The local structure in the cluster is the same between the two structures; however, the *P*-1 structure contains more pronounced terminal S−Au−S disorder. The poor quality of the $P2_1/n$ structure did not allow for anisotropic refinement of the carbon atoms in the *t*-butyl thiol groups. In both structures,

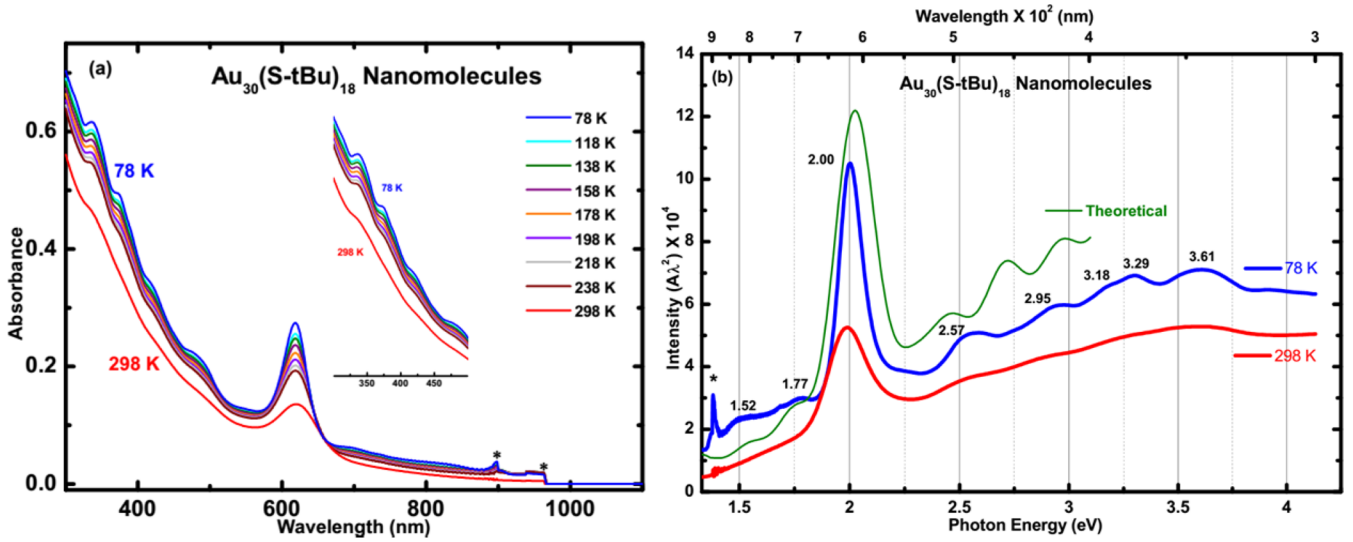

Figure 2. (a) Temperature-dependent UV−vis−NIR absorption spectra of $Au_{30}(S\text{-}tBu)_{18}$ nanomolecules in 3-methyl tetrahydrofuran solvent. (b) Temperature-dependent UV−vis−NIR $Au_{30}(S\text{-}tBu)_{18}$ nanomolecules plotted as photon energy where peaks marked by an asterisk show an intrumental artifact, compared with the simulated TDDFT/B3LYP spectra of $Au_{30}(S\text{-}CH_3)_{18}$ (in green).

the external solvent contents could not be identified and were removed utilizing the SQUEEZE[9] program as implemented in the program PLATON.[10]

Experiment: Optical Spectroscopy. UV−vis−NIR absorption response of $Au_{30}(S\text{-}tBu)_{18}$ is measured in 2-metyltetrahydrofuran at predetermined temperatures upon equilibrating at each temperature for 3−5 min as shown in Figure 2a. Temperature-dependent optical absorption spectra of the nanomolecules showed increased absorption features, with minimal shifts of absorption maxima and well-resolved new vibronic peaks at lower wavelengths (~300 to ~550 nm). In Figure 2b, absorption intensity spectra are plotted against photon energy, showing approximately five distinct peaks in the 2.25−3.75 eV range and two new peaks in the low-energy region.

Theory: Structural Analysis. Local geometry relaxation employing density-functional theory (DFT) and the Perdew−Burke−Ernzerhof (PBE) exchange-correlation (xc-) functional[11] were performed on the crystallographic determined structural model of $Au_{30}(S\text{-}tBu)_{18}$, reporting the full Cartesian coordinates in the Supporting Information. It is interesting to compare the $Au_{30}(S\text{-}tBu)_{18}$ atomistic arrangement here determined for the first time with that of the homologous $Au_{30}S(S\text{-}tBu)_{18}$ compound whose stoichiometry differs only by addition of a S atom, determined in previous work.[7] We recall that in the $Au_{30}(S\text{-}tBu)_{18}$ structure a Au_{20} prolate core is protected by two $Au_3(S\text{-}tBu)_4$ and four $Au(S\text{-}tBu)_2$ units and two bridge S-*t*Bu groups (see Figure 1). The insertion of an S anion on a hollow site of a Au_3 facet provokes a local swelling of the coordination environment, with the added S anion-like species pushing away the S atoms of one $Au_3(S\text{-}tBu)_4$ unit, while the other atoms approximately preserve their configuration, as can be appreciated by comparing Figures 4a and 4c (see especially the top part of the cluster). A previously proposed structural model of $Au_{30}(S\text{-}tBu)_{18}$ was obtained by erasing the added S atom in $Au_{30}S(S\text{-}tBu)_{18}$ and performing a local geometry relaxation,[7] a procedure which has been reproduced here and leads to the structure shown in Figure 4b. The local geometry relaxation maintains the swelling caused by the added S anion, so that in the structural model of Figure

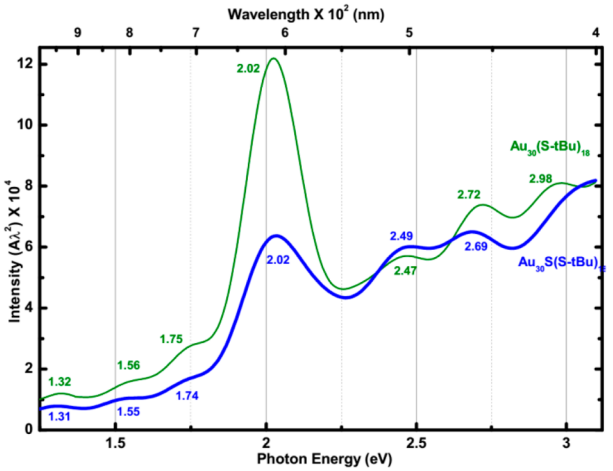

Figure 3. Theoretical UV−vis−NIR of $Au_{30}(S\text{-}tBu)_{18}$ and $Au_{30}S(S\text{-}tBu)_{18}$ nanomolecules plotted as photon energy.

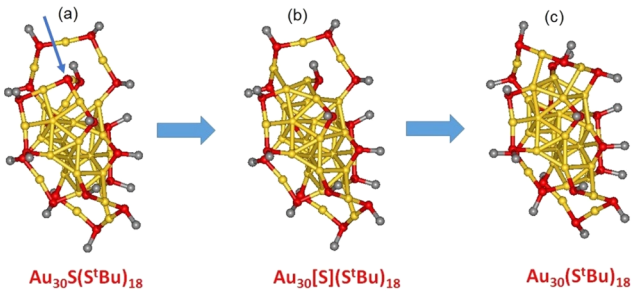

Figure 4. Schematic depiction of the clusters investigated in the present work: (a) $Au_{30}S(S\text{-}tBu)_{18}$ with an arrow highlighting the additional S atom; (b) $Au_{30}S(S\text{-}tBu)_{18}$ as obtained by a local relaxation of $Au_{30}S(S\text{-}tBu)_{18}$ after erasing the additional S atom; (c) $Au_{30}(S\text{-}tBu)_{18}$. The methyl groups are not shown for clarity of illustration.

4b one of the $Au_3(S\text{-}tBu)_4$ units is somewhat detached from the rest of the cluster. A more compact and thus energetically more favorable coordination (lower in energy by 0.39 eV) is restored in the $Au_{30}(S\text{-}tBu)_{18}$ crystal structure illustrated in Figure 4c,

proving the structural fluxionality of these monolayer-protected systems. Knowledge of the correct structure improves the comparison of experimental and simulated optical absorption spectrum, vide infra.

Theory: Optical Spectroscopy. The optical absorption spectrum of $Au_{30}(S\text{-}tBu)_{18}$ was simulated via time-dependent DFT (TDDFT) using two different xc-functionals: B3LYP[12] and SAOP[13] (see the Experimental section for more details). This allows us to compare the result of a hybrid (B3LYP) xc-functional and a semilocal Coulomb-corrected (SAOP) one, where a hybrid xc-functional is here employed to the best of our knowledge for the first time to predict the optical response of monolayer-protected clusters. To reduce the computational effort, in the TDDFT/B3LYP calculations the *t*Bu groups were replaced by CH_3 groups: this does not appreciably modify the absorption spectrum as proved in the SI using the SAOP approach. In Figure 2b the TDDFT/B3LYP spectrum is reported together with the experimental one. The agreement between experimental and simulated optical absorption spectra is excellent and is here improved by the use of the correct structural model with respect to previous work (see Figure 4a of ref 7). The intense peak at 2 eV in the experiment is predicted at 2.04 eV by theory, while minor features between 2.45 and 3 eV are also present which parallel the experimental ones in the same energy range. The TDDFT/SAOP spectrum is also reported in the Supporting Information and compares well with both the TDDFT/B3LYP and experimental spectra. As the TDDFT/B3LYP simulation is obtained by a real-time propagation of the electronic density, an analysis of the excitation components is not possible. This is instead readily available via the TDDFT/SAOP approach. Focusing on the band around 2 eV, which is the counterpart of the experimental peak at 620 nm in Figure 2a, we find that it is contributed by many discrete transitions (see Figure S5 in the Supporting Information), of which two are the most prominent:

- one at 1.92 eV with main single-particle components: 42% HOMO → LUMO+2; 18% HOMO−3 → LUMO; 14% HOMO−4 → LUMO
- one at 1.98 eV with main single-particle components: 43% HOMO → LUMO+4; 22% HOMO−5 → LUMO; 12% HOMO → LUMO+2

where HOMO is the highest-occupied molecular orbital and LUMO is the lowest-unoccupied molecular orbital. The molecular orbitals involved in such transition are illustrated in Figure 5. It is interesting to note that (i) the HOMO belongs essentially to the metal Au 6s band and therefore is very delocalized, (ii) the other occupied orbitals involved in the transitions (HOMO−3, HOMO−4, and HOMO−5) are more located on the Au−S bonds, with the 5d contribution the largest on the gold atom and the 3p contribution the largest on sulfur; (iii) the unoccupied orbitals mainly involved in the optical transitions (LUMO, LUMO+2, and LUMO+4) have a very similar nature: they are very delocalized over the central metal core gold atoms, with high Au 6s−6p contribution, with negligible contributions from Au 5d and small contributions from sulfur 3p. From this analysis we can ascribe the transitions involved in the main peak as excitations going from the Au−S bonds to the empty Au 6s−6p conduction band.

Finally in Figure 3 the TDDFT/B3LYP spectra of $Au_{30}(S\text{-}CH_3)_{18}$ and $Au_{30}S(S\text{-}CH_3)_{18}$ are compared, showing that interestingly the main differences between the optical properties of the two compounds lie in the main peak around 2 eV.

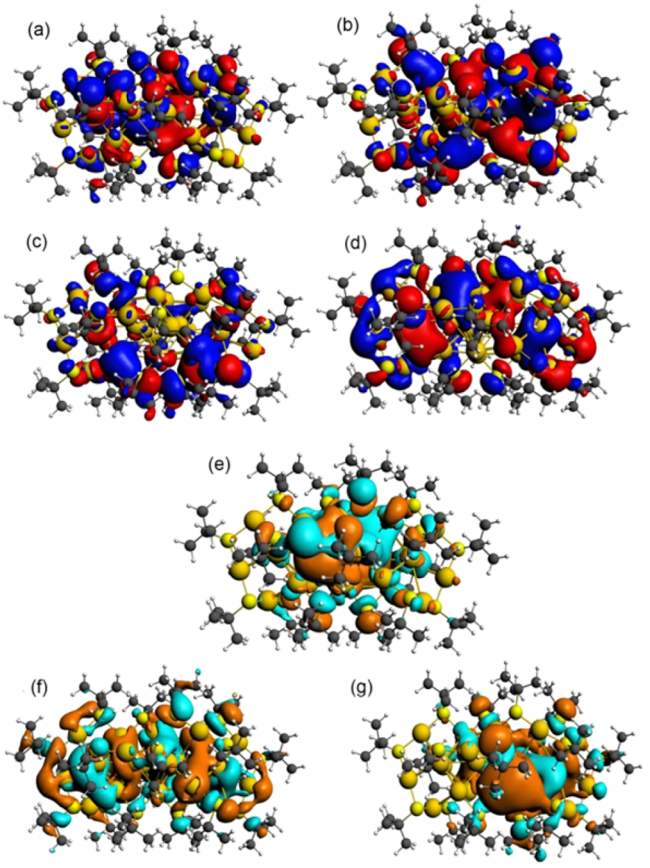

Figure 5. Plot of the orbitals mainly involved in the peak around 2 eV: (a) HOMO−5; (b) HOMO−4; (c) HOMO−3; (d) HOMO; (e) LUMO; (f) LUMO+2; (g) LUMO+4. Red/orange and blue/light-blue, respectively, correspond to opposite signs of the wave function. Red/blue and orange/light-blue correspond to occupied and virtual orbitals, respectively.

CONCLUSIONS

Determination of crystal structure of monolayer-protected gold clusters is a crucial step to achieve an in-depth understanding and control of the properties and functionalities of this class of materials. In the present work we were able to determine the crystallographic structure of $Au30(S\text{-}tBu)_{18}$, a compound exhibiting peculiar optical absorption in the visible region of the spectrum conferring it a characteristic color and making it a unique "green gold" species, whose structure had remained elusive until now despite that its presence in massive form had been demonstrated via mass spectrometric techniques. Structure determination then allows us to pursue a stringent comparison between theory and experiment for this species, from which three major conclusions can be drawn: (i) a great structural fluxionality with the existence of low-energy, subtly different isomers, (ii) an appreciable sensitivity of optical response to geometrical details, (iii) the possibility of achieving, through advanced computational tools, an excellent agreement between simulated and observed quantities. The present achievement opens the way to further investigations aimed at exploiting the unique optical features of this compound and tuning them to, e.g., biochemical and optoelectronic applications.

EXPERIMENTAL AND COMPUTATIONAL SECTION

Materials. Sodium borohydride (Acros, 99%), tertiary butylthiol (Acros, 99%), and *trans*-2-[3[(4-*tert*-butyl-phenyl)-2-methyl-2-propenylidene] malononitrile (DCTB matrix) (Fluka ≥99%) were purchased and used as received. HPLC grade solvents such as tetrahydrofuran, toluene, methanol, butylated hydroxytoluene, stabilized tetrahydrofuran, and acetonitrile were obtained from Fisher Scientific.

Synthesis. $Au_{30}(S\text{-}t\text{-}C_4H_9)_{18}$ nanomolecules were synthesized by reacting 0.1 g of $HAuCl_4{\cdot}3H_2O$ to 15 mL of HPLC grade THF, followed by addition of 87 μL of HS-*t*Bu (1:3 molar ratio) which was stirred at 450 rpm for 15 min. An excess of 12 mmol of $NaBH_4$ 0.113 g in 10 mL of cold H_2O was added. The reaction was stopped after 1 h and then washed with a combination of 5 mL of water and 40 mL of MeOH, three times. The crude product of 200 mg was combined with with 1 mL of toluene and 1 mL of HS-*t*Bu. The mixture of excess thiol and crude nanomaterial was etched at 70 °C for 4 h. After etching the product, it was washed again with a combination of 5 mL of water and 40 mL of MeOH, three times. SEC (size exclusion chromatography) was performed in order to separate $Au_{30}(S\text{-}t\text{-}C_4H_9)_{18}$ from the etched mixture. SEC was repeated 3−4 times to achieve ∼20 mg of pure $Au_{30}(S\text{-}t\text{-}C_4H_9)_{18}$.

Instrumentation. A matrix-assisted laser desorption time-of-flight (MALDI-TOF) mass spectrometer was used to acquire mass spectra with DCTB matrix on a Voyager DE PRO mass spectrometer. Compositional analysis was performed with electrospray ionization mass spectra (ESI-MS), collected from Waters Synapt HDMS using THF as the solvent. Temperature-dependent UV−vis-NIR absorption measurements were collected with an UV−vis−NIR Cary 5000 and JANIS VNF-100 low-temperature cryostat using 1-methyltetrahydrofuran as the solvent, and a Lakeshore Cyotronics temperature controller was used for temperature-dependent absorption measurements.

Single-Crystal X-ray Diffraction. Data for both $Au_{30}(S\text{-}t\text{-}Bu)_{18}$ structures ($P2_1/n$ and $P\text{-}1$) were collected on beamline 11.3.1 at the Advanced Light Source, Lawrence Berkeley National Laboratory. Samples were mounted on MiTeGen kapton loops and placed in a 100(2) K nitrogen cold stream provided by an Oxford Cryostream 800 Plus low-temperature apparatus on the goniometer head of a Bruker D8 diffractometer equipped with a PHOTON 100 CMOS detector operating in shutterless mode. Diffraction data were collected using synchrotron radiation monochromated using silicon(111) to wavelengths of 0.7293 and 0.7749 Å, respectively. An approximate full sphere of data was collected using a combination of phi and omega scans with scan speeds of 1 s per 4° for the phi scans and 3 and 5 s per degree for the omega scans at 2θ = 0 and −45, respectively. Additional crystallographic information has been summarized in the SI. Full details can be found in the crystallographic information files provided in the Supporting Information.

DFT Calculations. The optimized structure of the $Au_{30}(S\text{-}t\text{-}C_4H_9)_{18}$ complex was obtained starting from the experimentally determined geometry and performing a local relaxation. The Plane-Wave QuantumEspresso software[14] was adopted in conjunction with ultrasoft pseudopotentials[15] and the PBE xc-functional. Values of 30 and 300 Ry were used as the cut-offs for the selection of the plane wave basis sets for describing the kinetic energy and the electronic density, respectively. One-electron levels were broadened using a Gaussian distribution with σ = 0.002 Ry.

TDDFT Simulations. The TDDFT/B3LYP absorption spectra are the result of a real-time time-dependent DFT (RT-TDDFT) simulation, carried out with the CP2K package.[16] To reduce the computational effort, the CH_3 groups of the *tert*-butyl moieties were replaced with hydrogen atoms. DVZP primary basis set,[17] GTH pseudopotentials,[18] and an auxiliary cpFIT3 basis set as described in ref 19 were employed in the calculations. Starting from a ground-state calculation, optical response is obtained by subjecting the system to electrical pulses (with a strength of 0.0005 au) in each of the three Cartesian directions and using the time-evolution formalism to follow the electron dynamics. A total of 16.5 fs was sampled using a time step of 0.012 fs. A time damping of 7.3 fs was chosen to broaden the predicted spectrum. The TDDFT/SAOP spectra were calculated at the scalar relativistic ZORA[20]level, with the Amsterdam Density Functional (ADF) code[21,22] which solves the TDDFT equations with the Casida approach.[23]The basis set consists of all-electron Slater Type Orbitals (STO) of Triple Zeta plus Polarization (TZP) size for all the atoms, taken from the ADF ZORA database. SAOP exchange-correlation potential[13] was used, exhibiting a correct Coulombic asymptotic behavior. The 200 lowest eigenvalues of the Casida matrix were extracted. The discrete transitions have been convoluted with Lorentzian functions of 0.15 eV of fwhm. Using this less computationally demanding approach it is feasible to calculate TDDFT spectra using both $Au_{30}S(S\text{-}CH_3)_{18}$ and the original $Au_{30}(S\text{-}t\text{Bu})_{18}$ compound: the two spectra are compared in the SI and demonstrate that replacement of *t*Bu with methyl groups does not qualitatively alter the optical response of these species.

ASSOCIATED CONTENT

Supporting Information

Crystallographic data, detailed explanation of synthesis, pictorial representation of SEC performed on final etch product, ESI-MS of crude, etched, and final SEC product, ESI and MALDI mass spectra, Cartesian coordinates, experimental temperature-dependent UV−vis−NIR and simulated TDDFT/SAOP optical absorption spectra of $Au_{30}(StC_4H_9)_{18}$ and also $Au_{30}(SCH_3)_{18}$ for the simulated spectra. CCDC numbers are 1453205 (P-1) and 1453206 ($P2_1/n$) (PDF)

Crystallographic data files for $Au_{30}(S\text{-}t\text{-}Bu)_{18}$ (CIF)

AUTHOR INFORMATION

Corresponding Author

*E-mail: amal@olemiss.edu.

Notes

The authors declare no competing financial interest.

ACKNOWLEDGMENTS

We gratefully acknowledge the funding for experimental research from NSF-CHE-1255519. The Advanced Light Source is supported by the Director, Office of Science, Office of Basic Energy Sciences, of the U.S. Department of Energy under Contract No. DE-AC02-05CH11231. Computational research was performed in part using EMSL, a DOE Office of Science User Facility sponsored by the Office of Biological and

Environmental Research and located at Pacific Northwest National Laboratory, and PNNL Institutional Computing at Pacific Northwest National Laboratory.

REFERENCES

(1) Whetten, R. L.; Khoury, J. T.; Alvarez, M. M.; Murthy, S.; Vezmar, I.; Wang, Z. L.; Stephens, P. W.; Cleveland, C. L.; Luedtke, W. D.; Landman, U. Nanocrystal gold molecules. *Adv. Mater.* **1996**, *8* (5), 428−433.

(2) (a) Parker, J. F.; Fields-Zinna, C. A.; Murray, R. W. The Story of a Monodisperse Gold Nanoparticle: $Au_{25}L_{18}$. *Acc. Chem. Res.* **2010**, *43* (9), 1289−1296. (b) Heaven, M. W.; Dass, A.; White, P. S.; Holt, K. M.; Murray, R. W. Crystal structure of the gold nanoparticle $[N(C_8H_{17})_4][Au_{25}(SCH_2CH_2Ph)_{18}]$. *J. Am. Chem. Soc.* **2008**, *130* (12), 3754−3755. (c) Chaki, N. K.; Negishi, Y.; Tsunoyama, H.; Shichibu, Y.; Tsukuda, T. Ubiquitous 8 and 29 kDa gold: Alkanethiolate cluster compounds: Mass-spectrometric determination of molecular formulas and structural implications. *J. Am. Chem. Soc.* **2008**, *130* (27), 8608−8610. (d) Weissker, H. C.; Escobar, H. B.; Thanthirige, V. D.; Kwak, K.; Lee, D.; Ramakrishna, G.; Whetten, R. L.; López-Lozano, X. Information on quantum states pervades the visible spectrum of the ubiquitous $Au_{144}(SR)_{60}$ gold nanocluster. *Nat. Commun.* **2014**, DOI: 10.1038/ncomms4785.

(3) Offord, D. A.; John, C. M.; Linford, M. R.; Griffin, J. H. Contact Angle Goniometry, Ellipsometry, and Time-of-Flight Secondary Ion Mass Spectrometry of Gold Supported, Mixed Self-Assembled Monolayers Formed from Alkyl Mercaptans. *Langmuir* **1994**, *10* (3), 883−889.

(4) (a) Krommenhoek, P. J.; Wang, J.; Hentz, N.; Johnston-Peck, A. C.; Kozek, K. A.; Kalyuzhny, G.; Tracy, J. B. Bulky Adamantanethiolate and Cyclohexanethiolate Ligands Favor Smaller Gold Nanoparticles with Altered Discrete Sizes. *ACS Nano* **2012**, *6* (6), 4903−4911. (b) Nishigaki, J.-i.; Tsunoyama, R.; Tsunoyama, H.; Ichikuni, N.; Yamazoe, S.; Negishi, Y.; Ito, M.; Matsuo, T.; Tamao, K.; Tsukuda, T. A New Binding Motif of Sterically Demanding Thiolates on a Gold Cluster. *J. Am. Chem. Soc.* **2012**, *134* (35), 14295−14297. (c) Yang, H.; Wang, Y.; Edwards, A. J.; Yan, J.; Zheng, N. High-yield synthesis and crystal structure of a green Au30 cluster co-capped by thiolate and sulfide. *Chem. Commun.* **2014**, *50* (92), 14325−14327. (d) Hesari, M.; Workentin, M. S. Facile synthesis of $Au_{23}(SC(CH_3)_3)_{16}$ clusters. *J. Mater. Chem. C* **2014**, *2* (18), 3631−3638.

(5) (a) Nimmala, P. R.; Theivendran, S.; Barcaro, G.; Sementa, L.; Kumara, C.; Jupally, V. R.; Apra, E.; Stener, M.; Fortunelli, A.; Dass, A. Transformation of $Au_{144}(SCH_2CH_2Ph)_{60}$ to $Au_{133}(SPh\text{-}tBu)_{52}$ Nanomolecules: Theoretical and Experimental Study. *J. Phys. Chem. Lett.* **2015**, *6* (11), 2134−2139. (b) Nimmala, P. R.; Dass, A. $Au_{99}(SPh)_{42}$ Nanomolecules: Aromatic Thiolate Ligand Induced Conversion of $Au_{144}(SCH_2CH_2Ph)_{60}$. *J. Am. Chem. Soc.* **2014**, *136* (49), 17016−17023. (c) Nimmala, P. R.; Dass, A. $Au_{36}(SPh)_{23}$ Nanomolecules. *J. Am. Chem. Soc.* **2011**, *133* (24), 9175−9177. (d) Zeng, C.; Li, T.; Das, A.; Rosi, N. L.; Jin, R. Chiral Structure of Thiolate-Protected 28-Gold-Atom Nanocluster Determined by X-ray Crystallography. *J. Am. Chem. Soc.* **2013**, *135* (27), 10011−10013.

(6) Crasto, D.; Dass, A. Green Gold: $Au_{30}(S\text{-}t\text{-}C_4H_9)_{18}$ Molecules. *J. Phys. Chem. C* **2013**, *117* (42), 22094−22097.

(7) Crasto, D.; Malola, S.; Brosofsky, G.; Dass, A.; Häkkinen, H. Single Crystal XRD Structure and Theoretical Analysis of the Chiral $Au_{30}S(S\text{-}t\text{-}Bu)_{18}$ Cluster. *J. Am. Chem. Soc.* **2014**, *136* (13), 5000−5005.

(8) Gutierrez, E.; Powell, R. D.; Furuya, F. R.; Hainfeld, J. F.; Schaaff, T. G.; Shafigullin, M. N.; Stephens, P. W.; Whetten, R. L. Greengold, a giant cluster compound of unusual electronic structure. *European Physical Journal D* **1999**, *9* (1−4), 647−651.

(9) van der Sluis, P.; Spek, A. L. *Acta Crystallogr., Sect. A: Found. Crystallogr.* **1990**, *46*, 194−201.

(10) Spek, A. L. *J. Appl. Crystallogr.* **2003**, *36*, 7−13.

(11) Perdew, J. P.; Burke, K.; Ernzerhof, M. Generalized Gradient Approximation Made Simple. *Phys. Rev. Lett.* **1996**, *77* (18), 3865−3868.

(12) (a) Becke, A. D. Density-functional thermochemistry. III. The role of exact exchange. *J. Chem. Phys.* **1993**, *98* (7), 5648−5652. (b) Stephens, P. J.; Devlin, F. J.; Chabalowski, C. F.; Frisch, M. J. Ab Initio Calculation of Vibrational Absorption and Circular Dichroism Spectra Using Density Functional Force Fields. *J. Phys. Chem.* **1994**, *98* (45), 11623−11627.

(13) Gritsenko, O. V.; Schipper, P. R. T.; Baerends, E. J. Approximation of the exchange-correlation Kohn−Sham potential with a statistical average of different orbital model potentials. *Chem. Phys. Lett.* **1999**, *302* (3−4), 199−207.

(14) Giannozzi, P.; et al. QUANTUM ESPRESSO: a modular and open-source software project for quantum simulations of materials. *J. Phys.: Condens. Matter* **2009**, *21* (39), 395502.

(15) Vanderbilt, D. Soft self-consistent pseudopotentials in a generalized eigenvalue formalism. *Phys. Rev. B: Condens. Matter Mater. Phys.* **1990**, *41* (11), 7892−7895.

(16) Lippert, G.; Hutter, J.; Parrinello, M. The Gaussian and augmented-plane-wave density functional method for ab initio molecular dynamics simulations. *Theor. Chem. Acc.* **1999**, *103* (2), 124−140.

(17) VandeVondele, J.; Hutter, J. Gaussian basis sets for accurate calculations on molecular systems in gas and condensed phases. *J. Chem. Phys.* **2007**, *127* (11), 114105.

(18) Hartwigsen, C.; Goedecker, S.; Hutter, J. Relativistic separable dual-space Gaussian pseudopotentials from H to Rn. *Phys. Rev. B: Condens. Matter Mater. Phys.* **1998**, *58* (7), 3641−3662.

(19) Guidon, M.; Hutter, J.; VandeVondele, J. Auxiliary Density Matrix Methods for Hartree−Fock Exchange Calculations. *J. Chem. Theory Comput.* **2010**, *6* (8), 2348−2364.

(20) van Lenthe, E.; Baerends, E. J.; Snijders, J. G. *J. Chem. Phys.* **1993**, *99*, 4597−4610.

(21) Baerends, E. J.; Ellis, D. E.; Ros, P. Self-consistent molecular Hartree—Fock—Slater calculations I. The computational procedure. *Chem. Phys.* **1973**, *2* (1), 41−51.

(22) Fonseca Guerra, C.; Snijders, J. G.; te Velde, G.; Baerends, E. J. Towards an order-N DFT method. *Theor. Chem. Acc.* **1998**, *99* (6), 391−403.

(23) Cadsida, M. E. In *Recent Advances in Density-Functional Methods*; Chong, D. P., Ed.; World Scientific: Singapore, 1995; p 155.